

A Machine-Learning Framework for Design for Manufacturability

Aditya Balu^a, Sambit Ghadai^a, Gavin Young^a, Soumik Sarkar^a, Adarsh Krishnamurthy^{a,*}

^a*Department of Mechanical Engineering
Iowa State University
Ames, IA, USA*

Abstract

Computer-aided Design for Manufacturing (DFM) systems play an important role in reducing the time taken for product development by providing manufacturability feedback to the designer while a particular component is being designed. Traditionally, DFM rules are hand-crafted and used to accelerate the engineering product design process by integrating manufacturability analysis during design. Such a practice relies on the experience and training of the designer to create a complex component that is manufacturable. However, even after careful design, the inclusion of certain features might cause the part to be non-manufacturable. In this paper, we present a novel framework that uses machine-learning with computer-aided design (CAD) models to provide feedback about manufacturability. We use GPU-accelerated algorithms to convert standard boundary representation (B-rep) CAD models into volume based representations that can be directly used for machine-learning. Our framework uses 3D-Convolutional Neural Networks (3D-CNN) to learn the representative geometric characteristics that classify *difficult-to-manufacture* features in a CAD model of a mechanical part and determine if the part can be manufactured or not. As a proof of concept, we apply this framework to assess the manufacturability of drilled holes. CAD models with different manufacturable and non-manufacturable drilled holes are generated using a solid modeling kernel and then converted into volume representations using GPU-accelerated algorithms. This data is used to train a 3D-CNN for manufacturability classification. We visualize the feature-space of the 3D-CNN to understand the learning capability of the network in the context of manufacturable features. The framework has an accuracy of more than 78% in consistently classifying the manufacturable and non-manufacturable models. We further study the ability of the framework to identify *difficult-to-manufacture* features in parts that have multiple holes or more complicated than the CAD models used for training the network. Finally, the framework can explain the reason for non-manufacturability in a part using a gradient-based class activation map that can identify the *non-manufacturable* feature, and provide feedback to the designer about possible modifications.

Keywords: Machine Learning, 3D Convolution Network, DFM, GPU Algorithms, Voxelized Representation, Distance Fields

1. Introduction

The widespread adoption of computer-aided design (CAD) and computer-aided manufacturing (CAM) have resulted in the acceleration of the product development process, reducing the time taken to design a product [35]. However, the product development process, for the most part, is still decentralized with the design and manufacturing reviews being performed independently, leading to differences between the the *as-designed* and the *as-manufactured* component. A successful product needs to meet its specifications, while also being manufacturable. In general, the design engineer ensures that the product is able to function according to the specified requirements, while the manufacturing engineer gives feedback to the design engineer about its manufacturability. This iterative process is often time consuming, leading to longer product development times and higher costs. Recent researches in integrating design

and manufacturing [25, 35] have tried to reduce these differences and making the product development process easier and accessible to designers, who may not be manufacturing experts. In addition, there have been different efforts to enable a collaborative product development process and reduce the number of design iterations [31, 5, 6]. However, with the increase in complexity of designs, integrating the manufacturability analysis within the design environment provides an ideal solution to improve the product design process.

Current CAD/CAM systems have facilitated integration of design and manufacturing, which have been further unified with the use of cloud computing [11] and product lifecycle management systems [32]. However, successful product design still relies on the experience of the designer to create manufacturable designs. Design for manufacturing (DFM) analysis [10] can help in integrating this manufacturing experience to CAD systems, with the help of handcrafted rules that can be used to improve the manufacturability of the design. The process of creation of the DFM rules themselves is usually based on empirical observations and is specific to the manufacturing process rather than the design itself. Hence, it has been shown that successful application of DFM requires prior knowledge of manufac-

*Corresponding Author

Email addresses: baditya@iastate.edu (Aditya Balu), sambitg@iastate.edu (Sambit Ghadai), gyoungis@iastate.edu (Gavin Young), soumiks@iastate.edu (Soumik Sarkar), adarsh@iastate.edu (Adarsh Krishnamurthy)

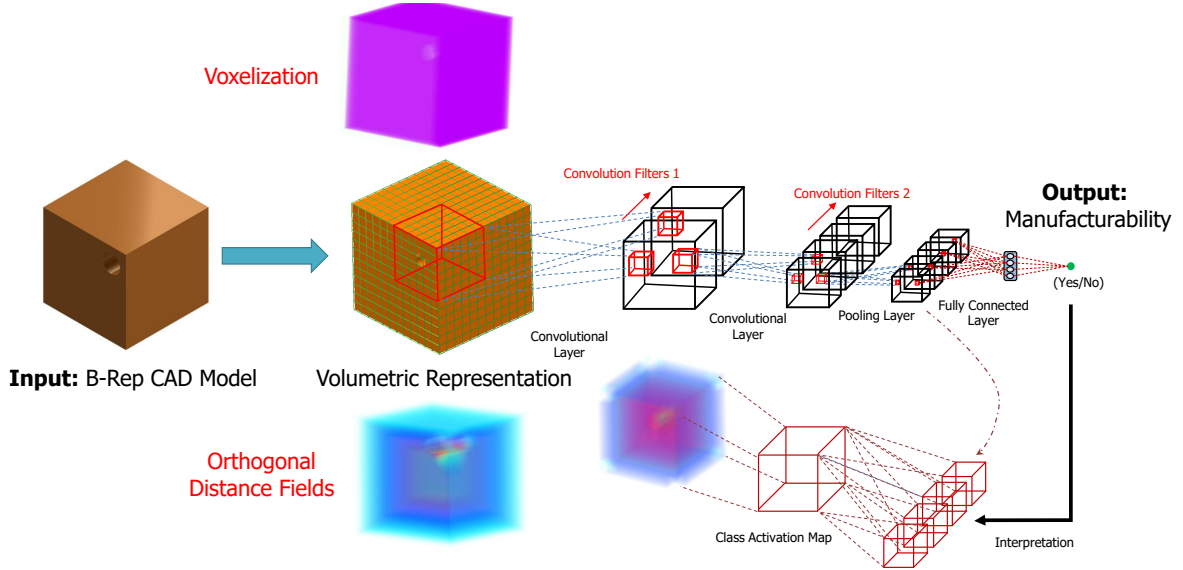


Figure 1: Framework for deep-learning based design for manufacturability. The CAD model is converted into volume representations and is input to the 3D convolutional neural network (3D-CNN) for manufacturability classification. The 3D-CNN output is analyzed to provide manufacturability feedback.

turing. In addition, thinking about the design in a practical and structured manner produces better manufacturable designs [33]. Hence, ideally, the next generation CAD systems need to have cognitive capabilities [7]; they need to have built-in intelligence for analyzing manufacturability in a practical and structured manner. In this paper, we develop a machine-learning based decision-support framework for cyber-enabled manufacturing, which can be used to ensure the manufacturability of a design during the design process.

Among various machine learning techniques, deep learning (DL) methods are particularly suitable for building a cognitive CAD system due to their hierarchical feature learning capability without explicit hand-crafting. They are designed to automatically learn complicated features in a hierarchical manner directly from available data [17]. In addition to being extensively used in computer vision [18, 20, 16], deep learning is also gaining popularity within the engineering community, especially in prognostics [19, 1], engineering design [21, 8], and robotic path planning [22]. The hierarchical architecture of deep learning can be used to learn progressively complex features by capturing *features of features*. Thus, our Deep Learning based Design for Manufacturing (DLDFM) framework can be used to learn the different DFM rules from different examples of manufacturable and non-manufacturable components without explicit handcrafting (Figure 1). In addition, the *learned* network can be integrated with CAD systems, providing interactive feedback about the manufacturability of the design and assisting in removing manufacturability barriers in design [25]. Finally, the framework can also identify the source of non-manufacturability, which can then be suitably modified by the designer to make the overall design manufacturable.

For the DL algorithms to identify *non-manufacturable* features, the CAD model of the component needs to be suitably represented. The CAD representation needs to be compatible

with the hierarchical learning capability of DL algorithms to interpret the results in a sensible manner. Traditional mechanical CAD systems represent the geometry using boundary representation (B-rep) for ease of rendering. In B-rep, the geometry of a solid model¹ is represented using only its boundary entities (for example, faces in 3D). However, there is no information that corresponds directly to the volume or material contained within a solid model. As a result, it will be challenging to build a DL algorithm that can directly learn spatial attributes from a B-rep. In addition, it would be difficult to interpret any features that are learned by a DL algorithm directly from B-rep. Volume representations, on the other hand, are much more suitable for DL algorithms, especially 3D-convolutional neural networks (3D-CNNs). In our framework, we convert the CAD models from B-rep to volumetric representations, specifically voxelizations and orthogonal distance fields. These representations allow the framework to learn the *non-manufacturable* features and can also be used to identify them on further analysis of the network.

In this paper, we introduce a novel machine learning framework for design for manufacturability that uses deep learning (3D-CNN) to learn the DFM rules and identify *non-manufacturable* features. The main contributions of this paper include:

- GPU-accelerated methods for converting B-rep solid models to volume representations (binary voxelization and orthogonal distance fields).
- A deep-learning based DFM framework to analyze the manufacturability of drilled hole in a CAD geometry.
- A novel voxel-wise gradient-weighted feature localization based on the DLDFM framework to visualize *non-*

¹Note: In this paper, we focus only on solid models, which are 2-manifold with a well defined interior and exterior.

manufacturable features and provide manufacturability feedback to the designer.

This paper is arranged as follows. We explain the volume representations that we use for DL in Section 2. We describe the GPU-accelerated algorithms that convert B-reps to the volume representations in Section 3. In Section 4, we provide the details of the DLDFM framework, including generating the datasets that are used for training and testing the 3D-CNN. In Section 5, we discuss the details of the 3D-CNN, including the network architecture and the hyper-parameters. Finally, in Section 6, we show the results of the DLDFM framework in classifying *manufacturable* and *non-manufacturable* features and the learning capability of the framework.

2. Volume Representations for Machine Learning

Conventional models in traditional CAD systems use B-rep to represent the solid models using the set of faces that bound the model. However, using B-rep makes it difficult to identify features that might be *difficult-to-manufacture*. In our framework, we convert the B-rep CAD models to a volumetric representation.

2.1. Voxelization

The use of voxelized shape representation allows a digital representation of the CAD model, where each voxel of the model can be represented using a binary digit corresponding to the voxel being inside or outside the model. Using this method, the entire model can be represented using a long string of binary digits that can be used as input for training the machine learning network. A 2D example of the representation is shown in Figure 2.

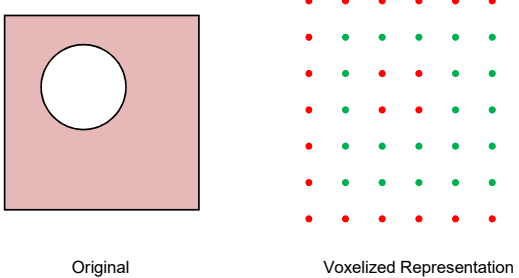


Figure 2: Visualization of 2D voxelized CAD model. The voxels marked in red are outside the model while the voxels marked in green are inside.

However, the voxelized data is still limited in its capability to represent the solid model. The voxelized representation of the CAD model contains only digital information of whether the corresponding voxel is inside or outside the model. It does not have information about the proximity of a voxel to the boundary. In addition, as shown in Figure 3, the voxelized representation does not contain any information about the distance between features. However, the proximity of other features or the boundary might be important in determining the manufacturability of a part. Hence, we augment our voxelized data with distance information.

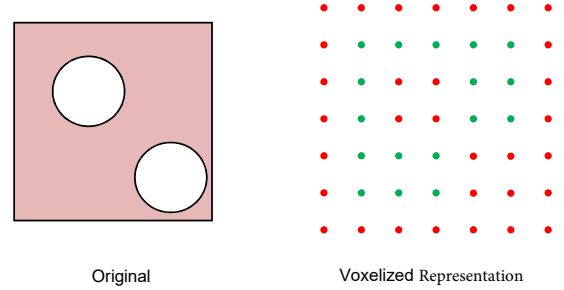


Figure 3: Limitations of binary voxelized approach. The CAD model on the left has 2 holes and its voxelized representation is shown on the right. There is no information of the proximity of the hole to the boundary. In addition, the information about its proximity to the other hole is also not available.

2.2. Orthogonal Distance Field Representation

To overcome the limitation of voxelized representations, the CAD model can be represented using distance fields. In a discretized distance field representation, each voxel inside the model stores the distance to the closest boundary of the model. Distance fields are commonly used in computer vision, path planning, and scientific visualization applications [14]. Using distance fields provide additional information about the proximity of a voxel to the closest boundary.

Given a point $q \in \mathcal{S}$, a solid model that is bounded by $d\mathcal{S}$ in \mathbb{R}^3 , the distance field D can be mathematically represented using the equation:

$$D = \min(\text{dist}(q, p)) \mid q \in \mathcal{S}, p \in d\mathcal{S}. \quad (1)$$

Even though there are efficient methods to compute the distance fields [14], computing the accurate minimum distance values for all $q \in \mathcal{S}$ is computationally expensive. This problem is exacerbated in a machine learning framework, where thousands of models need to be converted to the distance field representation for training the DL network. Fortunately, the machine learning framework can still learn from approximate but consistent distance information. Hence, to accelerate the conversion from B-reps to distance representations for training, we develop a new approximate distance field representation called orthogonal distance fields. We compute the distance from each point in the solid model to the closest boundary in the six orthogonal directions ($+x, -x, +y, -y, +z, -z$). This can be mathematical represented using the equation:

$$D_{\text{ortho}} = \min(\text{dist}(q, p)) \mid q \in \mathcal{S}, p \in d\mathcal{S}_{\text{ortho}}^q, \quad (2)$$

where $d\mathcal{S}_{\text{ortho}}^q$ is a subset of $d\mathcal{S}$. $d\mathcal{S}_{\text{ortho}}^q$ is the union of sets $d\mathcal{S}_x^q$, $d\mathcal{S}_y^q$, and $d\mathcal{S}_z^q$, given by,

$$d\mathcal{S}_x^q = \{p \mid \forall p \in d\mathcal{S}, p_y = q_y, p_z = q_z\}, \quad (3)$$

$$d\mathcal{S}_y^q = \{p \mid \forall p \in d\mathcal{S}, p_x = q_x, p_z = q_y\}, \quad (4)$$

$$d\mathcal{S}_z^q = \{p \mid \forall p \in d\mathcal{S}, p_x = q_x, p_y = q_y\}. \quad (5)$$

This computation is significantly less expensive and can be accelerated using the GPU as shown in Section 3.2.

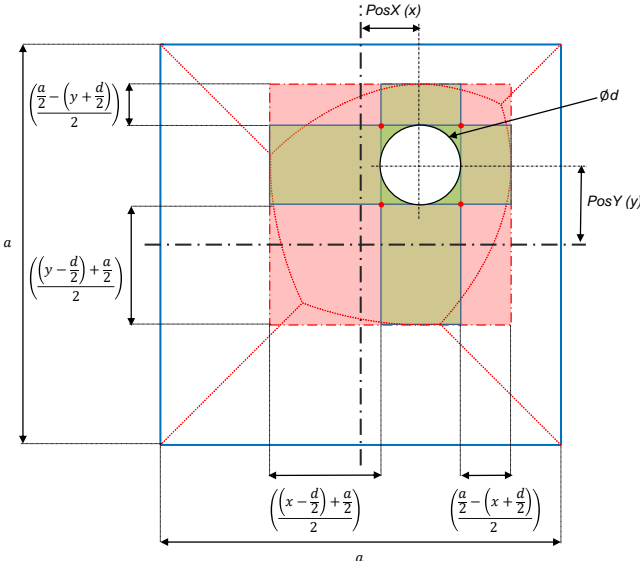


Figure 4: Orthogonal distance field for a Square with a hollow circle. The four rectangles in pink color represents the region with significant approximation.

Even though, it represents the exact distance fields for simple geometries such as a cuboid, it deviates significantly when the object includes any non-convex edges. For example, consider a square with a hollow circle inside as shown in Figure 4. In this case there are a few regions (marked in red) where the closest boundary to the point is the circle, but the orthogonal distance fields compute the minimum distance from the edge of the square. The bounds to the area of this region can be calculated as

$$A_I = \frac{(a - d)^2}{4}. \quad (6)$$

In addition, there are regions (marked in green) where the closest boundary is correctly identified, but the distance computed using orthogonal distance fields is different than the correct shortest distance. The maximum deviation between the orthogonal distance and the shortest distance occurs at the corners of the red rectangles (marked with a red dot). The area of this green region is

$$A_{II} = \left(\left(\frac{\pi}{4} - 1 \right) d + a \right) d \quad (7)$$

There is a C^0 discontinuity in the orthogonal distance fields at the intersection of the two (green and red) regions. This discontinuity can be smoothed in a discrete voxel mesh using Gaussian filters. In addition, they can be convolved with linear filters to obtain the correct distance fields [26]. A layer of the 3D-CNN has the capability to learn the weights and filters to perform this operation. Hence, an appropriately tuned 3D-CNN using orthogonal distance fields should have a similar performance to a different 3D-CNN that uses the correct distance fields. Hence, our machine learning framework can be trained to identify the salient features of a circular hole using the orthogonal distance fields. In the next section, we discuss the GPU-accelerated computation of the voxelized and the orthogonal distance field representation.

3. Computing Volume Representations from B-reps

We have developed methods for accelerated computation of volume representation of CAD models using graphics processing units (GPUs). These GPU methods are more than 10x faster than existing state-of-the-art CPU-based methods and can create a volumetric representation of a CAD model with more than 250,000,000 voxels. This high-resolution representation would have sufficient resolution to capture small features in CAD models. We construct a fine grid in the region occupied by the object using its axis-aligned bounding box. The B-rep model is then decomposed into its component surfaces, which is tessellated into triangles with a very fine resolution that is less than one-tenth of the resolution of the volumetric grid.

3.1. Voxelization

We make use of a rendering-based approach to classify the voxel centers as being inside or outside the geometry [13]. Using this method on the GPU, a fine voxelization of the model (up to 750 million voxels) with a relative voxel size of 0.001, can be generated (Figure 6).

The CAD model is rendered slice-by-slice by clipping it while rendering. The model is rendered to an off-screen framebuffer once for each slice to classify the voxelization. Each pixel of this clipped model is then used to classify the voxel corresponding to the slice as being inside or outside the CAD model. This is performed by counting the number of fragments

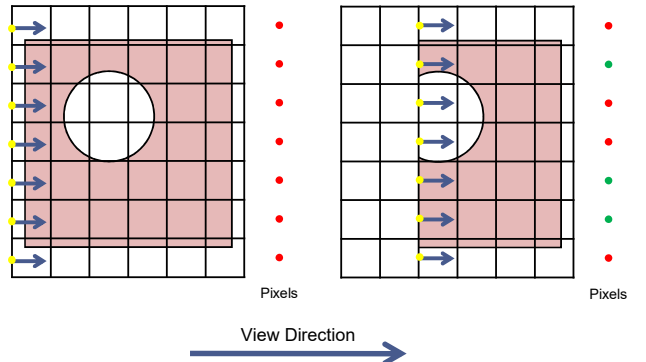


Figure 5: Performing voxelization in 2D using GPU rendering. A clipped CAD model is rendered slice-by-slice and the the number of rendered pixels is counted. The pixels that are rendered an odd number of times in each slice are inside the object (green).

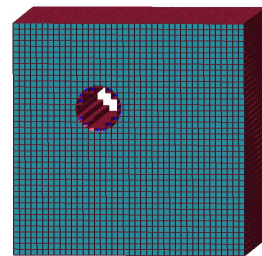


Figure 6: Example of a voxelized 3D CAD model. The voxels that make up the model are rendered as boxes.

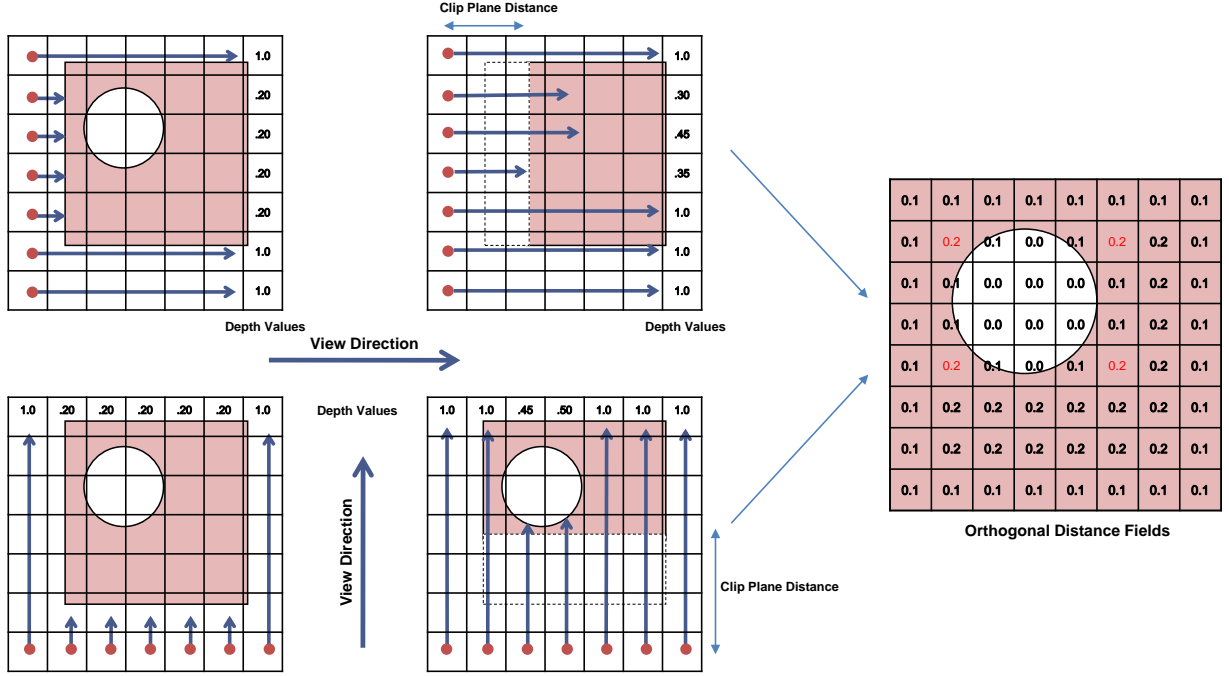


Figure 7: Performing orthogonal distance field computation in 2D using GPU rendering. A clipped CAD model is rendered slice-by-slice and the depth of the closest pixel fragment is stored. Finally, the minimum depth value from all the four orthogonal directions in 2D (only 2 shown here) at each pixel is computed as the orthogonal distance field.

that were rendered in each pixel using the stencil buffer on the GPU. After the clipped model has been rendered, an odd value in the stencil buffer indicates that the voxel on the particular slice is inside the CAD model, and vice versa (Figure 2). The process is then repeated by clipping the model with a plane that is offset by the voxel size. Once all the slices have been classified, we can get the complete voxelized representation of the CAD model.

The time taken to perform the classification is the sum of the time taken to tessellate the model once and the total time taken to render each slice. As an example, the total time taken to voxelize the hole block is 0.133 seconds. These timings are obtained by running our voxelization algorithm on a Intel Xeon CPU with 2.4 GHz processor, 64 GB RAM, and an NVIDIA Quadro K2200 GPU.

3.2. Orthogonal Distance Fields

We use an approach similar to the voxelization approach in Section 3.1. The CAD model is rendered using orthographic projection to an off-screen framebuffer slice-by-slice by clipping it while rendering. The depth values for each pixel of this clipped model, stored in the depth buffer, is then used to get the orthogonal distance value for each pixel in the slice. After the clipped model has been rendered, the normalized depth values are read from the depth buffer (Figure 7).

The normalized depth values read from the depth buffer corresponds to the closest boundary along the specified orthogonal direction in which the model is rendered. However, this depth value is measured from the near plane of the projection. Hence, the depth values need to be adjusted with the distance of the

model clipping plane from the near plane, to get the distance to the closest orthogonal boundary. After rendering all the slices, the depth to the closest orthogonal boundary is stored in each voxel for this particular direction. Similarly, depth information for all the six directions are obtained. The orthogonal distance field is then obtained by taking the minimum of the six distance values. The orthogonal distance fields for a simple cube with a hole rendered using volume rendering is shown in Figure 8.

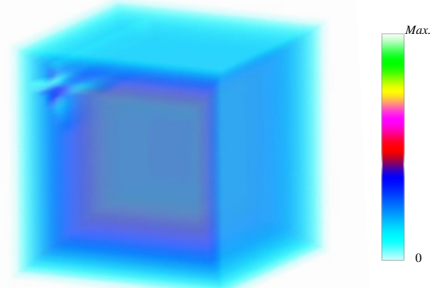


Figure 8: Volume rendering of the orthogonal distance field of a 3D CAD model. The color represents the distance to the boundary. Moving further inside the object represents a larger distance to the boundary, and the color changes from blue to red.

The time taken to compute the distance fields is the sum of the time taken to evaluate each of the 6 directional distance fields. As an example, the total time taken to compute the orthogonal distance fields for a cubical block with hole is 0.177 seconds. These timings are obtained by running our orthogo-

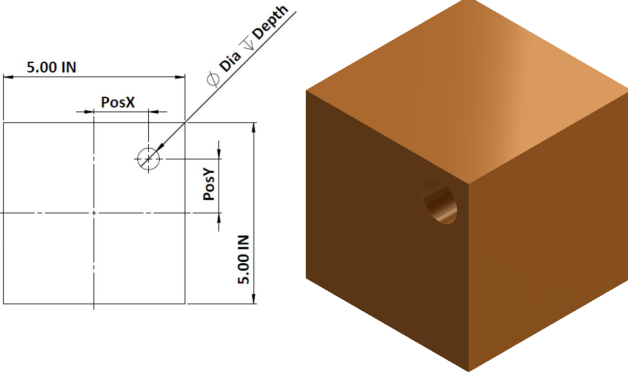


Figure 9: A sample block with a drilled hole with its dimensions highlighted in the projected view.

nal distance fields computation algorithm on a Intel Xeon CPU with 2.4 GHz processor, 64 GB RAM, and an NVIDIA Quadro K2200 GPU.

4. Deep Learning Based Design for Manufacturing

The objective of the design process is to design products that meet the specifications of the functional requirements, while being able to be manufactured in a cost-efficient manner. Often, the manufacturing process and parameter selection is itself an optimization problem [9]. Thus, understanding the constraints for the design space requires more information about the manufacturing processes, which makes the concurrent engineering process difficult and manual.

DFM guidelines were developed by design and manufacturing researchers to make the design process compliant with manufacturing [2]. In addition, researchers used these DFM guidelines to develop manufacturability analysis systems (MAS), which take into account the rules provided by the DFM guidelines to analyze the manufacturability of the part [29]. Many MAS frameworks require the parameters of the part as additional user input, to analyze the manufacturability of the part. These MAS frameworks then use the knowledge base of different DFM rules to provide manufacturability feedback. In addition, there are very few interactive parametric 3D solid modeling tools that provide manufacturability feedback to the designer, and enable changes to the design for improving manufacturability [28]. In this paper, we demonstrate the utility of a DLDFM tool in analyzing the manufacturability of a product design without any prior knowledge about the manufacturing process. We show a proof-of-concept of the DLDFM framework for drilling operations.

4.1. DFM Rules for Drilling

DFM rules for drilling have been developed based on the parameters of the cylindrical geometry as well as the geometry of the stock. The important geometric parameters are the diameter of the hole, the depth of the hole, and the position of the hole. However, there are certain additional parameters that might affect the training of the machine learning framework, but do not

contribute to the manufacturability analysis. For example, the face of the stock on which the hole is to be drilled does not affect the manufacturability of the hole, but need to be considered while training because the volumetric representation of the CAD model is not rotationally invariant.

In our DLDFM framework, the following DFM rules are considered to classify the drilled hole as manufacturable.

- 1. Depth-to-diameter ratio:** It is difficult to maintain the accuracy of the hole at greater depths for a given diameter. In addition, at greater depths it is possible for the tool to experience high loads sufficient enough to break the drill. Though the manufacturability of the hole for a particular part depends further on the tool material and the workpiece material, a general rule established for all machinable materials is used here. The depth-to-diameter ratio should be less than 5.0 for the machinability of the hole. [2, 3]
- 2. Through holes:** The rule for drilling a through hole changes because a through hole can be drilled from both directions. Hence, the depth-to-diameter ratio for a through hole should be less than 10.0 to be manufacturable.
- 3. Holes close to the edges:** Holes which are close to the edge are considered non-manufacturable because the thin sections near the edge usually collapse while manufacturing. A generic rule that a manufacturable hole must be surrounded with material of thickness at least equal to the half the diameter of the hole is used.
- 4. Thin sections in the depth direction of the hole:** Similar to the previous rule and also considering the geometry of the drill, it is not possible to drill a deep hole that leaves a thin section of material in the depth direction of the hole. Hence, a rule that any hole with difference in the stock length in the depth direction and depth of the hole greater than half the diameter is manufacturable.

The preceding rules are used to generate the ground truth manufacturability data for the training set, which is then used to learn the manufacturable and non-manufacturable features by the DLDFM Framework. However, it should be noted that for a DLDFM framework, one need not explicitly mention the rule. Rather, for industrial applications, one can train the DLDFM framework using the industry relevant historical data available in the organization, which need not be strictly rule based. The historical data can also be based on experience during previous attempts to manufacture a part. Thus, this DLDFM framework is an attempt to generate a DFM framework based on few basic rules. For more complicated shapes, one can just augment the training set and then re-train the DLDFM framework, which can then be used for analyzing complex parts for manufacturability. This eliminates the factor of expertise of the manufacturing engineer, which is one of the major advantages of having a cognitive DFM-CAD system. Thus, a designer with no knowledge of manufacturing can design manufacturable parts.

4.2. Training Data

Based on the DFM rules for drilling, different sample solid models are generated using a CAD modeling kernel. We use

ACIS [30], a commercial CAD modeling kernel to create the solid models. A cubical block of edge length 5.0 inches with different sizes of drilled holes are created (Figure 9). The diameter of the hole is varied from 0.1 in. to 1.0 in. with an increment of 0.1 in. Similarly, the depth of the hole is varied from 0.5 in. to 5.0 in. with an increment of 0.5 in. In addition, few geometries are specifically generated with thin sections in the depth direction to make the training data complete. The holes are generated at different positions on the face of the cube by varying the value of $PosX$ and $PosY$ (Figure 9). For sake of simplicity, the holes are located only along the diagonal of the drilling face, i.e. $PosX = PosY$ for all the training samples generated. In addition, the holes are generated in all the six faces of the cube. It should also be noted that the through holes are not generated on the six faces, but only on three faces, to avoid redundancy in the training data. After the CAD models are generated using the solid modeling kernel, they are classified for manufacturability using the DFM rules for drilled holes.

After the B-rep models are generated using the CAD modeling kernel, they are converted to volume representations, voxelization and orthogonal distance fields. One of the framework design choices is to choose an appropriate voxel grid for the model. A fine voxelization of the model, while capturing all the features accurately, might be computationally expensive for training the 3D-CNN. Even a voxelization resolution of $64 \times 64 \times 64$ pushes the limits of the GPU and CPU memory, and hence, the parameters of the 3D-CNN have to be tuned for optimal performance.

4.3. Representative and Non-Representative Models

For machine learning, the volumetric representation of CAD geometries (described in Section 4.2) are used for training the DLDFM network. During the training phase of DLDFM, there are many hyper-parameters (discussed in detail in Section 4) that need to be fine-tuned for optimal learning. For this reason, the data is split into a training set and a validation set. The training set is used to train the parameters of the DLDFM network, while the validation set is used to find the optimal hyper-parameters for the DLDFM.

In order to test the performance of the DLDFM network, a new test set of CAD models are generated. The CAD geometry generated in this set is different from the CAD models used in training the DLDFM. Further, we split the test set into two classes, representative and non-representative.

Representative models are broadly defined as those geometries that are related to CAD models in the training set. For example, the DLDFM network was trained using models with a single hole on different faces and at different positions. The geometries in the test set that belong to this subset of the CAD model parameters are classified as representative geometries. However, the models generated in the representative set do not have the same depth or diameter values as those in the models of the training set. For the representative test data, the following parameters are varied to generate the samples.

- Diameter values from 1.1 to 1.5 are used for the representative test data. Diameter values from 0.1 to 1.0 inches

were used for training.

- Position of the holes is varied in the radial directions ($PosX = 0$ or $PosY = 0$, while the other is varied), as well as in the diagonal direction. The position of the hole vary only in the diagonal direction ($PosX = PosY$) in the training samples.

Non-representative models are broadly defined as those geometries that are completely different from the training set. Deep learning has the ability to generalize geometries and patterns associated with the input space. Deep learning networks do not strictly memorize the relationship between the input space and the output space, but rather create a mapping to the output space based on the features learned from the input model. Thus, given any geometry, if the feature is recognized by DLDFM, then it can predict the manufacturability of the geometry based on the recognized feature. This generalization ability can be tested by creating a non-representative test set, containing geometries with the same primary hole parameters (depth, diameter, and position of the hole), but having additional or different external features. The details of the geometries in the non-representative data set is given below.

Multiple holes: The DLDFM has been trained to analyze the manufacturability of a single drilled hole. However, in an a designed component, the features may not be independent; there can be multiple features, each of which may or may not be manufacturable. Moreover, it is possible that each of the features themselves are manufacturable, but due to their proximity or interaction with other features, the part may become non-manufacturable. Hence, we test the ability of the DLDFM framework to analyze the manufacturability of a part with two holes. It should be noted that the two holes in the same face and in different faces have different constraints on manufacturability. The non-representative data set contains both intersecting and non-intersecting holes with the additional manufacturability constraints as given below.

Holes in same face: When the two holes are on the same face, the manufacturability rules 1 and 2 defined previously in Section 4.1 apply to each hole independently. In addition, there is an interaction rule based on the relative position of the holes to each other. If the holes are too close, then the third rule in Section 4.1 applies based on the thickness of the region between the holes. This is to prevent the collapse of the thin section between the holes during manufacturing, making the part non-manufacturable.

Holes in different faces: We only consider non-intersecting holes on different faces. When the two holes are on different faces, the standard manufacturability rules 1 and 2 defined in Section 4.1 apply to each hole independently. When the holes are on perpendicular faces, but close enough to create a thin section between them, then rule 3 from Section 4.1 applies. Finally, when the holes are on opposite faces, and the axis of the holes are close enough to create a thin section in the depth direction, then rule 4 from Section 4.1 apply.

L-shaped Blocks: All the models in the training set have an external cubical shape. However, a cognitive DFM-CAD sys-

tem should be able to learn the manufacturability rules irrespective of the external geometry. Hence, to test the capability of DLDFM to capture the manufacturability of a hole irrespective of the external geometry, we use an L-shaped Block with holes on different faces. The rules established in Section 4.1 also apply to this geometry.

We generated 9531 CAD models in total for the training and validation set. Out of these, 75% of the models were used for training the 3D-CNN and the remaining 25% of the models were used for validation or fine-tuning the hyper-parameters of the 3D-CNN. A detailed description of the training process is provided in Section 5. The trained DLDFM network is then tested using the test set CAD models. The test set contains 675 representative geometries and 1090 non-representative geometries.

5. 3D-Convolutional Neural Networks for DFM

Convolutional neural networks (CNN) [15] are a natural candidate to learn salient features in a hierarchical manner from volumetric representations of CAD models. Currently, 3D-Convolutional Neural Networks (3D-CNN) have been used for 3D object recognition and detection problems [24, 23]. Traditionally, the 2D-Convolutional Neural Networks have been used for object classification and image segmentation. The key distinction between 3D-CNN and its 2D counterpart is that the convolutional filters used are three-dimensional. It has been shown that deep learning based approaches have a significantly higher accuracy in object recognition and detection than traditional approaches. Our DLDFM framework uses a 3D-CNN to analyze the manufacturability of CAD models.

3D-CNNs consist of three different kinds of layers: convolutional, pooling, and fully-connected layers (Figure 1). Each convolutional layer in a 3D-CNN consists of different filters, which convolve with the input to generate a set of activation maps. The next convolutional layer takes the output activation map of the previous layer and performs convolutions with a new set of filters to get a new activation map. Thus, given an input volumetric representation, the filters are convolved in a hierarchical manner, which enables the 3D-CNN to recognize complex features. The first convolutional layer usually contains primitive information about the edges, corners etc of the model. The next layer can combine this primitive information to obtain more complex information about the features of the model. The pooling layer of the 3D-CNN performs a sub-sampling operation. Subsampling the volumetric representation can allow the 3D-CNN to focus on larger features, while ignoring smaller features that might not affect the manufacturability of the part. The fully-connected layer combines the activations of all the feature-of-features from the last convolutional or pooling layer to generate the final manufacturability decision.

5.1. Network Architecture and Hyper-Parameters

Deciding the manufacturability of a part can be framed as a binary classification problem. The input to the 3D-CNN is a voxelized CAD model of size $64 \times 64 \times 64$. The input data

is either the *Binary Inside-outside* or the *Orthogonal Distance Field* representation. The input volumetric data is first padded with zeros before convolution is performed. Zero padding is necessary in this case to ensure that the information about the boundary of the CAD model is not lost while performing the convolution.

There are several hyper-parameters of the 3D-CNN that need to be tuned in order to ensure that the learning is optimal. These include: number of convolutional layers, number of pooling layers, number of filters in each convolutional layer, filter size for each layer, and subsampling of the pooling layer. The specific hyper-parameters used in our framework are listed in Section 6.

The specific approaches used to optimize the 3D-CNN used in our framework are briefly given below for completeness. The volumetric data, after zero padding, is convolved with different filters to obtain the feature maps. Each filter activation is obtained using Rectified Linear Units (ReLU),

$$h(x_i) = \max(0, x_i), \quad (8)$$

where x_i is the input and $h(x_i)$ is output activation. Each unit of the feature map is associated with a common shared weight or kernel for efficient learning. Convolutional layers are succeeded by a batch normalization layer to reduce covariance shifts and to avoid saturation of the activations. The 3D-CNN consists of a single output with sigmoid activation denoting the probability of the class being 0 (manufacturable) or 1 (non-manufacturable). The 3D-CNN parameters are optimized by error back-propagation with binary cross-entropy as the loss function [12] and using the ADADELTA optimizer [34].

5.2. Interpretation of 3D-CNN Output

The trained DLDFM network can be used to test the manufacturability of any new geometry and can be treated as a black-box. However, such an approach does not help the designer in understanding the source of the network output, or make suitable design modifications to the part that improves manufacturability. Hence, interpretability and explainability of the output are essential for cognitive CAD systems that provide manufacturability feedback. In this paper, we attempt to make the DLDFM more transparent by being able to visualize the input features that lead to a particular manufacturability decision. A similar approach was used in object recognition in images by using class activation maps to obtain class specific feature maps [27]. The class specific feature maps could be obtained by taking a class discriminative gradient of the prediction with respect to the feature map to get the class activation. In this paper, we present the first application of gradient weighted class activation map (3D-GradCAM) for 3D spatial applications.

In order to get the feature localization map using 3D-GradCAM, we need to compute the spatial importance of each feature map in the last convolutional layer of the DLDFM, for a particular manufacturability or non-manufacturability class. The mathematical formulation for computing the $L_{3DGradCAM}$ is given in Appendix A. The activations obtained for the input part can be analyzed using $L_{3DGradCAM}$ to identify the source of

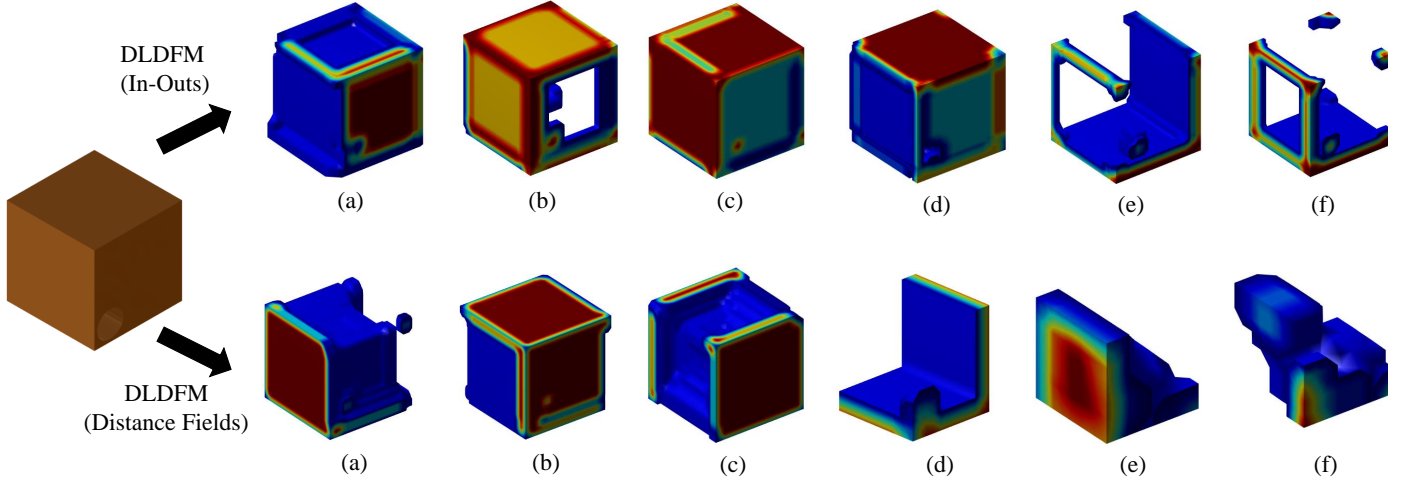


Figure 10: Feature map visualization with respect to the second (a, b, c) and the third (d, e, f) layers of the 3D-CNN trained using in-outs information (top row) and orthogonal distance fields (bottom row).

non-manufacturability. To spatially identify the source of non-manufacturability and render it, the heat map of ($L_{3DGradCAM}$) is resampled using linear interpolation to match the input size, and then overlaid in 3D with the input. This composite data is finally rendered using a volume renderer.

We make use of a GPU-based ray-marching approach to render this data. The rendering is parallelized on the GPU with each ray corresponding to the screen pixel being cast independently. The intersection of the ray with the bounding-cube of the volumetric data is computed, and then the 3D volumetric data is sampled at periodic intervals. The sum of all the sampled values along the ray is then computed. This value is converted to RGB using a suitable color-bar and rendered on the screen. Table 2 shows different volumetric renderings of the composite 3D-GradCAM data.

6. Results and Discussion

The different CAD geometries generated as explained in Section 4 are classified to be manufacturable or non-manufacturable based on the rules discussed in Section 4.1. The B-rep CAD geometries are converted to volumetric representation using voxelization and orthogonal distance field representation as explained in the Section 3. The grid size of $64 \times 64 \times 64$ is used for the volumetric representation in order to represent the geometry with sufficient resolution. We initially use the voxelized representation of the CAD geometry to train the DLDLFM network. Later, we use the orthogonal distance field representation of the CAD geometry to train another DLDLFM network.

6.1. Tuning of the Hyper-parameters

The hyper-parameters for the DLDLFM are fine-tuned to have least validation loss. The architecture of the network used is

shown in Table 3. A batch size of 60 is selected while training the DLDLFM network. The training was performed using Keras [4] in a Python environment. The DLDLFM network was trained in a workstation with a CPU RAM of 128GB, and a NVIDIA Titan X GPU with 12GB GPU RAM.

6.2. Visualization of the Features

The ability of the 3D-CNN to learn the features and hence, predict the manufacturability of a part can be understood by visualizing the feature maps. Figure 10 shows the output obtained from the second layer and third layer of the 3D-CNN. It can be seen that the 3D-CNN is able to recognize a few primitive information about the geometry; for example, the edges, the face, the hole in the cube, etc. Further, it can be observed that the next layer contains geometries of higher complexity.

6.3. Test Results

The DLDLFM network was first trained using the voxelized input (*in-outs* information only). After successful training, the DLDLFM network was tested on the representative test set to understand its performance. The *in-outs* based DLDLFM network performs well with an accuracy of 78% on 675 models of the representative test set. However, the performance of the network reduces by a small extent while testing on the non-representative test set as expected (Table 1). It is observed that the number of examples which are considered to be non-manufacturable in the non-representative test set are predicted to be manufacturable by the DLDLFM model (see false negative examples in Table 1). Among the different examples which the *in-outs* based DLDLFM network failed to predict correctly are cases where the hole is close to the boundary and hence, the network cannot determine if the part is manufacturable or not. This is one of the drawbacks of the *in-outs* representation of the CAD geometry. The information about the proximity of the voxels to the boundary is not available.

Test Data Type	Model Description	True Positive	True Negative	False Positive	False Negative	Accuracy
Representative (675 models - 408 Manufacturable)	In-outs Information	383	146	25	121	0.7837
	Distance Fields	370	200	38	67	0.8445
Non-Representative (1090 models - 484 Manufacturable)	In-outs Information	301	464	183	142	0.7018
	Distance Fields	274	503	210	103	0.7128

Table 1: Quantitative performance assessment of the DLDFM on representative and non-representative data sets.

Feature	DFM	DLDFM Prediction	CAD Model	3D-GradCAM Visualization
Single Hole	Manufacturable	Manufacturable		
Single through-hole	Non-Manufacturable	Non-Manufacturable		
Two Holes in different faces	Manufacturable	Manufacturable		
Two Holes	Non-Manufacturable	Manufacturable		
Two Holes	One Hole Manufacturable One Hole Non-Manufacturable	Non-Manufacturable (based on the single non-manufacturable hole)		
L-shaped block with hole	Non-Manufacturable	Non-Manufacturable		
L-shaped block with hole in the top face	Non-manufacturable	Non-manufacturable		

Table 2: Illustrative examples of manufacturability prediction and interpretation using the DLDFM framework.

DLDFM Network	Network Architecture
DLDFM with <i>in-outs</i> information	8 Convolution filters of size 8 Max. Pooling with subsampling size 2 8 Convolution filters of size 4 Max. Pooling with subsampling size 2 8 Convolution filters of size 2
DLDFM with <i>Orthogonal Distance Fields</i> information	8 Convolution filters of size 8 Max. Pooling with subsampling size 2 8 Convolution filters of size 6 Max. Pooling with subsampling size 2 8 Convolution filters of size 4 8 Convolution filters of size 2 Max. Pooling with subsampling size 2

Table 3: Hyper-parameters selection for different 3D-CNNs.

Hence, to overcome the drawback of *in-outs* based DLDFM network, a new DLDFM network was trained with the orthogonal distance fields representation. It can be seen that the predictions for the manufacturability improve in comparison with *in-outs* representation of the geometry. Specifically, there was a significant improvement in the accuracy (a gain of 6%) for predictions in the representative test set as shown in Table 1. The feature maps obtained from the DLDFM network using orthogonal distance fields is able to recognize the features (Figure 10) in spite of the approximations explained in Section 2.2. Furthermore, the number of examples that are falsely classified to be manufacturable using the *in-outs* is reduced by using the orthogonal distance fields in both the representative and non-representative test set.

6.4. Visualization of 3D-GradCAM

Using the trained DLDFM network, it is possible to obtain the localization of the feature activating the decision of the DLDFM as explained in the Section 5.2. The 3D-GradCAM renderings for various cases is shown in the Table 2. We have used 3D-GradCAM to visualize the results of various inputs such as manufacturable holes, non-manufacturable-holes, multiple holes in same face, holes in multiple faces of the cube, and L shaped block. 3D-GradCAM can localize the features that can cause the part to be non-manufacturable. For example, in Table 2, the fifth example from the top shows a CAD model with 2 holes of which one of them is non-manufacturable. The 3D-GradCAM rendering correctly identifies the non-manufacturable hole and as a result the DLDFM network also predicts that the part to be non-manufacturable. The feedback is helpful to understand which particular feature among various other features in a CAD geometry accounts for the non-manufacturability and possibly modify the design appropriately. Hence, our DLDFM framework can be used in a cognitive CAD system to provide interactive manufacturability feedback.

7. Conclusions and Future work

In this paper, we have developed a deep-learning-based DFM (DLDFM) framework for high-throughput cyber-enabled manufacturing. To the best of our knowledge, this is the first application of deep learning to learn a data-driven design for manufacturability framework which can recognize the features and then analyze the manufacturability of the part. In this paper, our DLDFM framework was able to successfully learn the complex DFM rules for drilling from volume representations of 3D CAD geometries. This makes our framework scalable to other machining processes, unlike the rule based DFM frameworks that change from process to process.

This paper also serves as a proof-of-concept to demonstrate the feasibility of using 3D-CNNs for manufacturing applications using a voxel-based approach. The DLDFM was able to learn features directly from the voxelized model, without any additional shape information. In addition, to provide more information about the proximity of the boundaries, we compute orthogonal distance fields. The DLDFM network developed using the orthogonal distance fields achieves a better accuracy in correctly classifying the manufacturability than using only the *in-outs* information.

We also eliminate the black box notion about artificial neural networks; the DLDFM framework provides feedback about the source of non-manufacturability. Using the feedback provided by the 3D gradient-weighted class activation map, an interactive decision-support system for DFM can be integrated with current CAD systems, which can provide real-time manufacturability analysis while the component is being designed. This would ultimately reduce the design time, leading to significant cost-savings.

References

- [1] Akintayo, A., Lore, K. G., Sarkar, S., Sarkar, S., 2016. Early detection of combustion instabilities using deep convolutional selective autoencoders on hi-speed flame video. International Journal of Prognostics and Health Monitoring.
- [2] Boothroyd, G., Dewhurst, P., Knight, W., 2002. Product Design for Manufacture and Assembly. M. Dekker.

[3] Bralla, J. G., 1999. Design for manufacturability handbook. McGraw-Hill.

[4] Chollet, F., 2015. Keras. <https://github.com/fchollet/keras>.

[5] Cutkosky, M. R., Engelmore, R. S., Fikes, R. E., Genesereth, M. R., Gruber, T. R., Mark, W. S., Tenenbaum, J. M., Weber, J. C., 1993. PACT: An experiment in integrating concurrent engineering systems. *Computer* 26 (1), 28–37.

[6] Fischer, G., Grudin, J., Lemke, A., McCall, R., Ostwald, J., Reeves, B., Shipman, F., 1992. Supporting indirect collaborative design with integrated knowledge-based design environments. *Human-Computer Interaction* 7 (3), 281–314.

[7] Goel, A. K., Vattam, S., Wiltgen, B., Helms, M., 2012. Cognitive, collaborative, conceptual and creative - four characteristics of the next generation of knowledge-based CAD systems: a study in biologically inspired design. *Computer-Aided Design* 44 (10), 879–900.

[8] Guo, X., Li, W., Iorio, F., 2016. Convolutional neural networks for steady flow approximation. In: *Proceedings of the ACM Knowledge, Discovery, and Data Mining Conference (KDD 2016)*. pp. 481–490.

[9] Gupta, A. K., Guntuku, S. C., Desu, R. K., Balu, A., 2015. Optimisation of turning parameters by integrating genetic algorithm with support vector regression and artificial neural networks. *The International Journal of Advanced Manufacturing Technology* 77 (1-4), 331–339.

[10] Gupta, S. K., Regli, W. C., Das, D., Nau, D. S., 1997. Automated manufacturability analysis: a survey. *Research in Engineering Design* 9 (3), 168–190.

[11] He, W., Xu, L., 2015. A state-of-the-art survey of cloud manufacturing. *International Journal of Computer Integrated Manufacturing* 28 (3), 239–250.

[12] Hinton, G. E., Salakhutdinov, R. R., 2006. Reducing the dimensionality of data with neural networks. *Science* 313 (5786), 504–507.

[13] Hsu, M.-C., Wang, C., Xu, F., Herrema, A. J., Krishnamurthy, A., 2016. Direct immersogeometric fluid flow analysis using B-rep CAD models. *Computer Aided Geometric Design* 43, 143 – 158.

[14] Jones, M. W., Baerentzen, J. A., Sramek, M., 2006. 3d distance fields: A survey of techniques and applications. *IEEE Transactions on visualization and Computer Graphics* 12 (4), 581–599.

[15] Krizhevsky, A., Sutskever, I., Hinton, G. E., 2012. Imagenet classification with deep convolutional neural networks. In: *Advances in Neural Information Processing Systems*. pp. 1097–1105.

[16] Larochelle, H., Bengio, Y., 2008. Classification using discriminative restricted Boltzmann machines. In: *Proceedings of the 25th international conference on Machine learning*. ACM, pp. 536–543.

[17] LeCun, Y., Bengio, Y., Hinton, G., 2015. Deep learning. *Nature* 521 (7553), 436–444.

[18] Lee, H., Grosse, R., Ranganath, R., Ng, A. Y., 2009. Convolutional deep belief networks for scalable unsupervised learning of hierarchical representations. In: *Proceedings of the 26th annual international conference on machine learning*. ACM, pp. 609–616.

[19] Liang, Y., Wu, D., Liu, G., Li, Y., Gao, C., Ma, Z. J., Wu, W., 2016. Big data-enabled multiscale serviceability analysis for aging bridges. *Digital Communications and Networks* 2 (3), 97–107.

[20] Lore, K. G., Akintayo, A., Sarkar, S., 2017. LLNet: A deep autoencoder approach to natural low-light image enhancement. *Pattern Recognition* 61, 650–662.

[21] Lore, K. G., Stoecklein, D., Davies, M., Ganapathysubramanian, B., Sarkar, S., 2015. Hierarchical feature extraction for efficient design of microfluidic flow patterns. In: *Proceedings of The 1st International Workshop on Feature Extraction: Modern Questions and Challenges, NIPS*. pp. 213–225.

[22] Lu, Y., Yi, S., Liu, Y., Ji, Y., 2016. A novel path planning method for biomimetic robot based on deep learning. *Assembly Automation* 36 (2), 186–191.

[23] Maturana, D., Scherer, S., 2015. 3D convolutional neural networks for landing zone detection from LiDAR. In: *IEEE International Conference on Robotics and Automation (ICRA)*. IEEE, pp. 3471–3478.

[24] Maturana, D., Scherer, S., 2015. VoxNet: A 3D convolutional neural network for real-time object recognition. In: *International Conference on Intelligent Robots and Systems (IROS)*. IEEE, pp. 922–928.

[25] McMains, S., 2006. Design for manufacturing feedback at interactive rates. In: *Proceedings of the Tenth ACM Symposium on Solid and Physical Modeling*. p. 239.

[26] Sanchez, M., Fryazinov, O., Fayolle, P.-A., Pasko, A., 2015. Convolution filtering of continuous signed distance fields for polygonal meshes. In: *Computer Graphics Forum*. Vol. 34. Wiley Online Library, pp. 277–288.

[27] Selvaraju, R. R., Das, A., Vedantam, R., Cogswell, M., Parikh, D., Batra, D., 2016. Grad-cam: Why did you say that? visual explanations from deep networks via gradient-based localization. *arXiv preprint arXiv:1610.02391*.

[28] Shugrina, M., Shamir, A., Matusik, W., 2015. Fab forms: customizable objects for fabrication with validity and geometry caching. *ACM Transactions on Graphics* 34 (4), 100.

[29] Shukor, S. A., Axinte, D., 2009. Manufacturability analysis system: Issues and future trends. *International Journal of Production Research* 47 (5), 1369–1390.

[30] Spatial Corporation, 2009. ACIS Geometric Modeler: User Guide. Version 20.0.

[31] Toye, G., Cutkosky, M. R., Leifer, L. J., Tenenbaum, J. M., Glicksman, J., 1994. SHARE: A methodology and environment for collaborative product development. *International Journal of Intelligent and Cooperative Information Systems* 3 (02), 129–153.

[32] Tuli, P., Shankar, R., 2015. Collaborative and lean new product development approach: a case study in the automotive product design. *International Journal of Production Research* 53 (8), 2457–2471.

[33] Yuan, J. T. J., Kong, K. Y., Parveen, H., Zhixiang, H., Rajasekaran, G., Behera, J. K., Sanaei, R., Otto, K. N., HölttäYÖttok, K., 2014. An overview of design cognition between experts and novices. In: *Proceedings of International Conference on Advanced Design Research and Education (ICADRE14)*. pp. 156–160.

[34] Zeiler, M. D., 2012. ADADELTA: an adaptive learning rate method. *arXiv preprint arXiv:1212.5701*.

[35] Zeng, Y., Horváth, I., 2012. Fundamentals of next generation CAD/E systems.

Appendix A. 3D-GradCAM Formulation

In order to get the feature localization map using 3D-GradCAM, we need to compute the spatial importance of each feature map A_l in the last convolutional layer of the DLDFM, for a particular class, c (c can be either non-manufacturability or manufacturability, for the sake of generality) in the classification problem. This spatial importance for each feature map can be interpreted as weights for each feature map; it can be computed as the global average pooling of the gradients back from the specific class of interest as shown in Eqn. A.2.

The cumulative spatial importance activations that contribute to the class discriminative localization map, $L_{3DGradCAM}$, is computed using

$$L_{3DGradCAM} = \text{ReLU} \left(\sum_l \alpha_l \times A^l \right), \quad (\text{A.1})$$

where α_l are the weights computed using

$$\alpha_l = \frac{1}{Z} \times \sum_i \sum_j \sum_k \frac{\partial y^c}{\partial A_{ijk}^l}. \quad (\text{A.2})$$

We can compute the activations obtained for the input part using $L_{3DGradCAM}$ to analyze the source of non-manufacturability. The heat map of $(L_{3DGradCAM})$ is resampled using linear interpolation to match the input size, and then overlaid in 3D with the input to be able to spatially identify the source of non-manufacturability.